KINETICS, CATALYSIS, AND REACTION ENGINEERING

Fractional Factorial Study of HCN Removal over a 0.5% Pt/Al_2O_3 Catalyst: Effects of Temperature, Gas Flow Rate, and Reactant Partial Pressure

Haibo Zhao,[†] Russell G. Tonkyn,[†] Stephan E. Barlow,[†] Charles H. F. Peden,[†] and Bruce E. Koel*[,‡]

Chemical Sciences Division, Pacific Northwest National Laboratory, P.O. Box 999, Richland, Washington 99352, and Department of Chemistry, 6 E. Packer Avenue, Lehigh University, Bethlehem, Pennsylvania 18015

Hydrogen cyanide (HCN) oxidation under lean conditions was studied on 0.5% Pt/Al_2O_3 catalysts. Fractional factorial design was used to determine which factors had significant effects on HCN conversion in these experiments. We conclude that reaction temperature and gas hourly space velocity (GHSV) had the most significant effects on HCN conversion, whereas no significant effects were caused by the presence of either nitric oxide (NO) or propene (C_3H_6). Then, a central composite design was used to study the effects of temperature and GHSV on HCN conversion, C_3H_6 conversion, and NO_x selectivity. On the basis of a second-order polynomial equation model, regression analysis was used to study the significance of each variable and derive equations for each response. This showed that there was a significant interaction between temperature and GHSV in HCN conversion. HCN conversion decreased at larger values of GHSV and increased at higher temperatures, up to a transition temperature that depends on the GHSV value. Temperature and gas hourly space velocity also strongly affect both C_3H_6 conversion and NO_x selectivity, but in these two cases, there is no significant interaction between temperature and GHSV. Contour plots of HCN conversion, C_3H_6 conversion, and NO_x selectivity versus temperature and GHSV were constructed from an analysis of the measured data, and these plots were then utilized to find optimum values of HCN conversion, C_3H_6 conversion, and NO_x selectivity over the range of conditions investigated. Conditions for optimum catalyst operation, described by high HCN conversion and low NO_x selectivity, are reported.

1. Introduction

Increasingly stringent environmental regulations have led to continuing research on reducing harmful exhaust emissions. One approach, using nonthermal plasmas combined with suitable catalysts, can produce high removal efficiencies of NO_x [NO (nitric oxide) and NO_2 (nitrogen dioxide)] from diesel exhaust gas. When the gas mixture following plasma treatment passes through Na−Y or Ba−Y zeolites, NO_2 is reduced to a mixture of N_2, N_2O (nitrous oxide), HCN (hydrogen cyanide), and NO.[1,2] Toxic HCN poses a threat to the general public and must be removed by passing the effluent over another downstream catalyst. One possible choice for this catalyst, Pt/Al_2O_3, is very efficient for hydrocarbon oxidation[3−7] and has also been studied extensively for CO oxidation.[9−11] The mechanisms for these oxidation reactions involve adsorption of oxygen on the surface of platinum metal. Adsorbed O atoms on platinum can even make this catalyst efficient for soot oxidation.[12] Other studies have also shown that NH_3 can be oxidized easily on Pt-based catalysts.[13−15] Because HCN molecules contain both carbon and nitrogen atoms in low oxidation states, Pt/Al_2O_3 catalysts should be active for the oxidation of HCN. Indeed, this was recently confirmed by Hoard et al.[2]

Diesel exhaust that exits a nonthermal plasma and zeolite catalyst reactor contains part-per-million quantities of HCN, NO, and hydrocarbons and trace amounts of unconverted NO_2, in addition to the primary components N_2, O_2, and H_2O. Many factors, apart from reaction temperature and gas hourly space velocity (GHSV), can affect subsequent HCN oxidation reactions under these conditions. For example, C_3H_6 (propene) strongly adsorbs on supported Pt catalysts and changes the surface reactivity dramatically.[16] NO reacts with HCN to produce N_2 and N_2O and also reacts with O_2 to produce NO_2.[17] Thus, it is important to determine the effects of the presence of these two molecules on HCN oxidation on Pt/Al_2O_3.

Conventional methods for conducting such multivariable experiments use a "one-factor-at-a-time" approach that consists of changing one variable and measuring the influence of this change while keeping the other variables constant. This is both labor-intensive and time-inefficient, and this method can actually give misleading results because it implies only a partial exploration of the experimental design field and ignores possible interactions between variables. Such limitations can be avoided by using factorial experimental design, and this approach has been widely used in chemistry research.[18−30] Because catalytic research usually involves many variables in preparing and testing catalysts, factorial experimental design is a particularly powerful method in elucidating the effects of each factor and optimizing a process.[25−30] The advantages of a factorial design method over a more conventional approach have been discussed by Box et al.[31] In particular, a statistically based catalyst design method enables one to build deductive and predictive models that relate primary preparation variables to innate physicochemical properties of the catalyst, reaction rate parameters, and ultimately

* To whom correspondence should be addressed. Tel.: 610-758-5650. Fax: 610-758-6555. E-mail: brk205@lehigh.edu.
[†] Pacific Northwest National Laboratory.
[‡] Lehigh University.

10.1021/ie048777e CCC: $33.50
Published on Web 01/07/2006

reactor design.[28] When many factors are involved, a full factorial design leads to a dramatic increase in the number of experimental runs. Even when a two-level factorial design is used, this is usually prohibitive in terms of time and expense. Fractional factorial designs reduce the total number of treatment combinations while preserving the basic factorial structure of the experiment. These designs use the "main-effects" principle to reduce the number of treatment combinations. Essentially, the main-effects principle states that main effects tend to dominate two-factor interactions, two-factor interactions tend to dominate three-factor interactions, and so on. A full 2^k factorial design, where k is the number of factors (parameters), allows all of the interactions to be estimated. As k increases, more and more of these interactions generally become less important. Fractional factorial designs "sacrifice" the ability to estimate higher-order interactions in order to reduce the number of treatment combinations. In the present study of HCN conversion over a Pt/Al_2O_3 catalyst, we use a fractional factorial design approach and consider the following parameters: reaction temperature, gas hourly space velocity (GHSV), and C_3H_6 and NO concentrations.

2. Experimental Methods

2.1. Materials and Procedures. A commercially available 0.5% Pt on Al_2O_3 catalyst (Alfa Aesar) was pretreated at 450 °C with 6% O_2 (UHP, Air Liquide) for 3 h, and then pure N_2 was flowed over the catalyst overnight. Mixtures of HCN (0.5%) and NO (0.5%) in N_2 were purchased from Scott Specialty Gases. A 3% C_3H_6 in He mixture was obtained from Air Liquide. Reaction experiments were carried out in a quartz, fixed-bed reactor with a 0.62-in. inner diameter. In a typical experiment, 30 ppm HCN plus 6% O_2 was mixed with controlled amounts of C_3H_6 and NO and flowed over the catalyst for 30 min, with N_2 making up the balance. A weight of 2.12 g of catalyst was loaded into the reactor, and this filled a volume of 1.98 cm^3. Catalyst pellets were uniform and cylindrical with a length and diameter of 0.13 in. The GHSV was determined from the standard flow rate of the gas divided by the catalyst bed volume.

The reactor was heated by a cylindrical ceramic fiber heater (Watlow). Mass flow controllers (MKS type 1179 A and Tylan model FC-260) were used to control and regulate the influent gases. After the gas constituents were combined and mixed in the gas manifold, a three-way valve allowed the gas stream to either enter the catalyst reactor or bypass the reactor entirely for influent gas calibration. The experimental apparatus is very similar to that used by Yoon et al.[1]

The effluent gas was continuously analyzed by an FTIR spectrometer (Nicolet Magna IR 560, Omnic QuantPad software) equipped with a heated, 2-m multiple-path gas cell and a liquid-nitrogen-cooled MCT detector. For each FTIR spectrum, 25 scans were collected at 0.5 cm^{-1} resolution. A typical FTIR spectrum is shown in Figure 1. Concentrations of HCN, NO, N_2O, NO_2, H_2O, CO, C_3H_6, and CO_2 were determined by taking calibration spectra and applying a method developed in-house for Omnic QuantPad software. The response of the FTIR spectrometer was extremely linear and reproducible at all concentrations between the detection limit and the saturation regime, as long as all interferences are identified. In addition, Omnic QuantPad software enables the extraction of concentration information from overlapping peaks, as long as calibration standards of both the molecule of interest and the interfering molecule are available. Additional, detailed information about the use of FTIR spectra for concentration determination can be found in the Omnic QuantPad software manual.

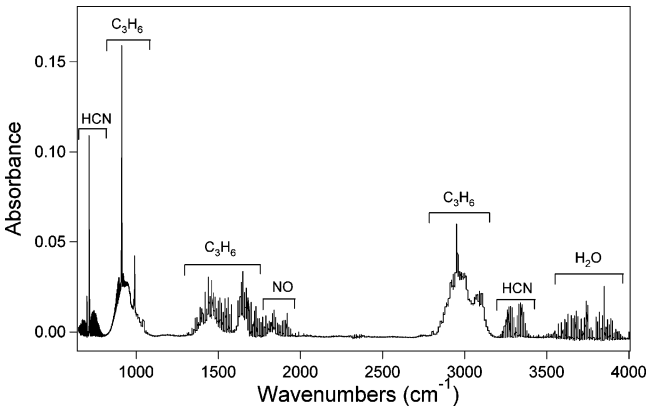

Figure 1. Typical FTIR spectrum used in concentration determinations.

Table 1. 2^{4-1} Fractional Factorial Design with Coded and Actual Independent Variables

	coded				actual			
run	X_1	X_2	X_3	X_4	x_1[a]	x_2[b]	x_3[c]	x_4[d]
1	−1	−1	−1	−1	90	13	165	30 300
2	+1	−1	−1	+1	504	13	165	87 870
3	−1	+1	−1	+1	90	52	165	87 870
4	+1	+1	−1	−1	504	52	165	30 300
5	−1	−1	+1	+1	90	13	277	87 870
6	+1	−1	+1	−1	504	13	277	30 300
7	−1	+1	+1	−1	90	52	277	30 300
8	+1	+1	+1	+1	504	52	277	87 870

[a] x_1: C_3H_6 concentration (ppm). [b] x_2: NO concentration (ppm). [c] x_3: temperature (°C). [d] x_4: gas hourly space velocity, GHSV (h^{-1}).

Table 2. Alias Structure in 2^{4-1} Fractional Factorial Design

I	$X_1X_2X_3X_4$
X_1	$X_2X_3X_4$
X_2	$X_1X_3X_4$
X_3	$X_1X_2X_4$
X_4	$X_1X_2X_3$
X_1X_2	X_3X_4
X_1X_3	X_2X_4
X_2X_3	X_1X_4

2.2. Statistical Design of Experiments. A 2^{4-1} fractional factorial design was used to study the main effects, as well as two-factor interaction effects, as a preliminary screen to identify the most important factors. The design in coded (X_i) and actual (x_i) independent variables is described in Table 1. The alias structure is shown in Table 2. The boundary conditions were as follows: x_1, C_3H_6 = 90−504 ppm; x_2, NO = 13 −52 ppm; x_3, temperature = 165−277 °C; and x_4, GHSV = 30 300−87 870 h^{-1}). In Table 2, the defining interaction is $I = X_1X_2X_3X_4$. Each main effect was aliased with the other three-factor interactions, and each two-factor interaction was aliased with the other two-factor interaction. Because C_3H_6 and NO had no significant effect on the total HCN conversion (see below), their concentrations were fixed at 250 and 30 ppm, respectively, in the following optimization experiments. These concentrations were chosen to be in the middle of the range used in our experiments, and they also represent typical concentrations of C_3H_6 and NO after our hydrocarbon-selective catalytic reduction (HSCR) of NO_x over oxide-based catalysts in lean exhaust. The "central composite design"[32] was then used to study the main effects of temperature and GHSV, and their interaction, on HCN conversion, C_3H_6 conversion, and NO_x selectivity. NO_x selectivity is defined as the ratio of the NO_x concentration in the effluent to the NO_x concentration in the feed, i.e., $NO_{x,OUT}/NO_{x,IN}$. Within the central composite design, we utilized the face-centered-cube design. Regression equations were developed

Table 3. Effects from 2^{4-1} Fractional Factorial Design with the Defining Relation $I = X_1X_2X_3X_4$[a]

run	mean	$X_1(X_2X_3X_4)$	$X_2(X_1X_3X_4)$	$X_3(X_1X_2X_4)$	$X_4(X_1X_2X_3)$	$X_1X_2(X_3X_4)$	$X_1X_3(X_2X_4)$	$X_2X_3(X_1X_4)$	HCN conversion
1	+1	−1	−1	−1	−1	+1	+1	+1	0.585
2	+1	+1	−1	−1	+1	−1	−1	+1	0.159
3	+1	−1	+1	−1	+1	−1	+1	−1	0.204
4	+1	+1	+1	−1	−1	+1	−1	−1	0.400
5	+1	−1	−1	+1	+1	+1	−1	−1	0.857
6	+1	+1	−1	+1	−1	−1	+1	−1	0.951
7	+1	−1	+1	+1	−1	−1	−1	+1	0.950
8	+1	+1	+1	+1	+1	+1	+1	+1	0.840
SUM+	4.946	2.35	2.394	3.598	2.06	2.682	2.58	2.534	
SUM−	0	2.596	2.552	1.348	2.886	2.264	2.366	2.412	
overall SUM	4.946	4.946	4.946	4.946	4.946	4.946	4.946	4.946	
difference	4.946	−0.246	−0.158	2.25	−0.826	0.418	0.214	0.122	
effect	0.61825	−0.0615	−0.0395	0.5625	−0.2065	0.1045	0.0535	0.0305	

[a] X_1, C_3H_6 concentration (ppm); X_2, NO concentration (ppm); X_3, temperature (°C); X_4, GHSV (h^{-1}).

that highlight the effects of temperature and GHSV, and their relative importance, on the HCN oxidation reaction. We also obtained information on the interaction between temperature and GHSV, which is not possible in a more traditional experimental design.

3. Results and Analysis

3.1. Main Effects and Two-Factor Interactions from a 2^{4-1} Fractional Factorial Design. A 2^{4-1} fractional factorial design was used to determine the main effects and two-factor interactions for the factors of C_3H_6 concentration, NO concentration, temperature, and GHSV on HCN conversion. A table of contrast was used to estimate the significance of these factors. The specific levels (lowest and highest values), HCN conversion, and calculated effects are listed in Table 3. In this table, SUM+ stands for total HCN conversion with + in that column, and SUM− stands for total HCN conversion with − in that column. Overall SUM denotes the sum of the SUM+ and SUM− values for that column, and difference denotes the difference in value between SUM+ and SUM− in that column. Effect is a value that characterizes the sensitivity of the system to the factors within the design.[32] Because eight experiments or experimental runs were carried out, the effect value for the mean column was calculated by dividing the difference value in that column by 8, and the other effect values were obtained by dividing the difference value in the same column by 4.

The effect values in Table 3 show that X_3 (temperature) had the most significant, positive main effect on HCN conversion. HCN conversion increased rapidly with an increase in reaction temperature between 165 and 277 °C. Because HCN oxidation is an exothermic process, raising the reaction temperature will decrease HCN conversion if it is a thermodynamically limited process. Our results show that HCN oxidation under these conditions is a kinetically controlled process. Raising the temperature helps to overcome the reaction barrier, which increases the reaction rate and thereby improves HCN conversion. X_4 (GHSV) has the most negative main effect on HCN conversion. In other words, HCN conversion decreased when the GHSV was increased. This result is not surprising, because the residence time of the reactants decreases when the GHSV is increased. The other two factors, X_1 (C_3H_6 concentration) and X_2 (NO concentration), had very small, negative main effects that were not significant in comparison to those of temperature and GHSV. The large excess of O_2 in the feed gas might enable NO and C_3H_6 oxidation reactions to persist in parallel with HCN oxidation without much interference.

The only significant interaction effects involved temperature and GHSV, and this interaction has a positive effect on HCN conversion. Because we found that the C_3H_6 and NO concentrations had only a small effect on HCN conversion, we focused the rest of our study on the effects of temperature and GHSV while keeping the C_3H_6 and NO concentrations at constant values.

3.2. Response Function. The dependence of the HCN conversion on temperature and GHSV is cast mathematically as a response function, R. It is simplest to first use the coded variables X_i, and we utilized a polynomial equation based on a Taylor series expansion, which can be written for two factors as

$$R = \beta_0 + \beta_3X_3 + \beta_4X_4 + \beta_{33}X_3^2 + \beta_{44}X_4^2 + \beta_{34}X_3X_4 + \cdots \quad (1)$$

where the coefficients β_i give the importance of each term. Here, higher-order terms are omitted. We included second-order terms because the response for most processes display curvature in the neighborhood of the optimal settings, and strict first-order models provide no way to account for this curvature.

The values of the coded variables X_i needed for this equation are calculated from the actual measured values of the variables x_i by using the expression

$$X = \frac{x - \frac{(x_{high} + x_{low})}{2}}{\frac{(x_{high} - x_{low})}{2}} \quad (2)$$

where x_{high} and x_{low} are the boundary conditions. In our experiment, these values are 287 and 165 °C, respectively, for the temperature factor and 90 900 and 30 300 h^{-1}, respectively, for the GHSV factor. X_3 (temperature) and X_4 (GHSV) are calculated as

$$X_3 = \frac{x_3 - 226}{61} \quad (3)$$

and

$$X_4 = \frac{x_4 - 60\,600}{30\,300} \quad (4)$$

In addition, one should have a sound strategy for taking the experimental data in order to best evaluate this response function. We utilized a face-centered design[32] approach.

3.2.1. Effects of Temperature and GHSV on HCN Conversion. Results for HCN conversion, C_3H_6 conversion, and NO_x selectivity based on experimental conditions given by a

Table 4. Factors and Levels for a Face-Centered Design[a]

	coded		actual		HCN	C_3H_6	NO_x
run	X_3	X_4	x_3	x_4	conversion	conversion	selectivity
1	−1	−1	165	30 300	0.452	0.267	0.692
2	+1	−1	287	30 300	0.949	0.928	1.016
3	−1	+1	165	90 900	0.175	0.058	0.92
4	+1	+1	287	90 900	0.855	0.798	1.090
5	−1	0	165	60 600	0.235	0.134	0.668
6	+1	0	287	60 600	0.894	0.854	0.397
7	0	−1	226	30 300	0.934	0.893	0.881
8	0	+1	226	90 900	0.663	0.583	1.084
9	0	0	226	60 600	0.782	0.716	0.554
10	0	0	226	60 600	0.785	0.716	0.553
11	0	0	226	60 600	0.784	0.711	0.549

[a] C_3H_6 and NO concentrations were set at 250 and 30 ppm, respectively.

Table 5. Regression Analysis for HCN Conversion

predictor[a]	coefficient	standard deviation	*t* ratio	*p*
constant	0.777 68	0.015 57	49.94	0.000
X_3	0.306 00	0.012 39	24.69	0.000
X_4	−0.107 00	0.012 39	−8.63	0.000
X_3^2	−0.204 21	0.019 07	−10.71	0.000
X_4^2	0.029 79	0.019 07	1.56	0.179
X_3X_4	0.045 75	0.015 18	3.01	0.030

Analysis of Variance

source	DF	SS	MS	*F*	*p*
regression	5	0.746 19	0.14924	161.93	0.00
error	5	0.004 61	0.00092		
total	10	0.750 79			

source	DF	SEQ SS
X_3	1	0.561 82
X_4	1	0.068 69
X_3^2	1	0.105 06
X_4^2	1	0.002 25
X_3X_4	1	0.008 37

[a] $s = 0.030\ 36$, $R^2 = 99.4\%$, R^2(adj) = 98.8%.

face-centered design are presented in Table 4. The center run was repeated three times in our experiments.

First, we consider in this section the dependence of HCN conversion on temperature and GHSV. This is done using the response function given in eq 1 for the effects of these factors on HCN conversion. A regression analysis was done to evaluate the β_i values. The analysis of variance (ANOVA) table[32] generated by MINITAB Statistical Software (Minitab, Inc., State College, PA; version 10) is listed in Table 5. The *p* value[32] in Table 5 was used to judge the significance level of each term. It is common to label the term as insignificant if the *p* value is larger than 0.05.[32] For HCN conversion, tests on individual coefficients suggest that all of the terms except X_4^2 are at least marginally significant. After dropping X_4^2, a new regression analysis was done with MINITAB. The output from this analysis is given in Table 6. The regression equation for HCN conversion (y_1) can now be given as

$$y_1 = 0.790 + 0.306X_3 - 0.107X_4 - 0.196X_3^2 + 0.0458X_3X_4 \quad (5)$$

Table 6 shows an R^2 value of 99.1%, which indicates that our model explains 99% of the total variability, which is excellent. Also, Table 6 shows that, over the range of temperatures and GHSV values studied in our experiments, these two factors have only weak interaction effects on the measured value of HCN conversion.

The HCN conversion function is shown in Figure 2 as a contour plot of eq 5 after X_3 and X_4 have been replaced by eqs 3 and 4. This function displays some curvature in its dependence on temperature, which is explained by the polynomial term of the temperature factor in eq 5. A significant result of this analysis is that Figure 2 can be used to estimate HCN conversion at any temperature and GHSV within the experimental regime. It also shows the limitations placed on the total HCN conversion by the GHSV value. For example, HCN conversion cannot reach 90% at 70 000 h^{-1} GHSV, regardless of the reaction temperature. One also can see that the conversion of HCN increases with increasing temperature before a transition temperature where the HCN conversion reaches a maximum, which depends on the value of GHSV. For a value of 6.56×10^4 h^{-1} GHSV, the transition temperature is 273 °C. Above the transition temperature, there is no good physical reason for the "rollover" (i.e., decrease in HCN conversion) shown in these curves at high temperature, and so we attribute this to a curve-fitting artifact. Other data (not utilized here) on HCN conversion at different temperatures with GHSV at 30 300 h^{-1} show that HCN conversion approaches a constant number around 95%.[17] This result suggests that our modeling of HCN conversion could be improved by taking more data near the transition temperature, in the range of 260−290 °C.

Table 6. Regression Analysis for HCN Conversion after Dropping X_4^2

predictor[a]	coefficient	standard deviation	*t* ratio	*P*
constant	0.789 60	0.015 12	52.23	0.000
X_3	0.306 00	0.013 80	22.17	0.000
X_4	−0.107 00	0.013 80	−7.75	0.000
X_3^2	−0.196 27	0.020 47	−9.59	0.000
X_3X_4	0.045 75	0.016 90	2.71	0.035

Analysis of Variance

source	DF	SS	MS	F	*p*
regression	4	0.743 94	0.185 98	162.76	0.00
error	6	0.006 86	0.001 14		
total	10	0.750 79			

source	DF	SEQ SS
X_3	1	0.561 82
X_4	1	0.068 69
X_3^2	1	0.105 06
X_3X_4	1	0.008 37

[a] $s = 0.033\ 80$, $R^2 = 99.1\%$, R^2(adj) = 98.5%.

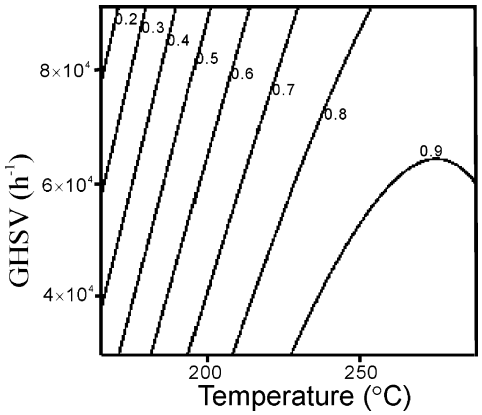

Figure 2. Contour plot of HCN conversion versus temperature and GHSV.

Figure 2 and eq 5 provide very useful information for designing processes for catalytic removal of HCN. For example, our results indicate that new parameters need to be optimized to improve HCN conversion if diesel engine exhaust has to be run over the catalyst at a high value of GHSV. These parameters

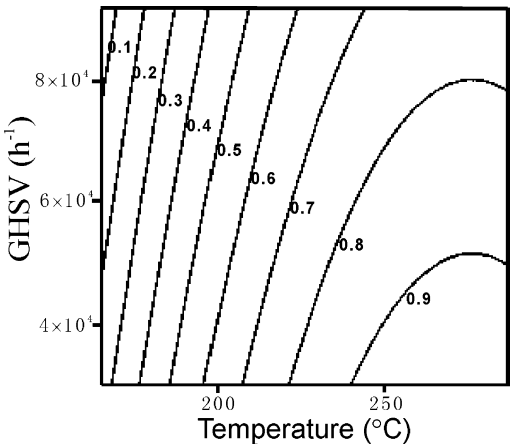

Figure 3. Contour plot of C_3H_6 conversion versus temperature and GHSV.

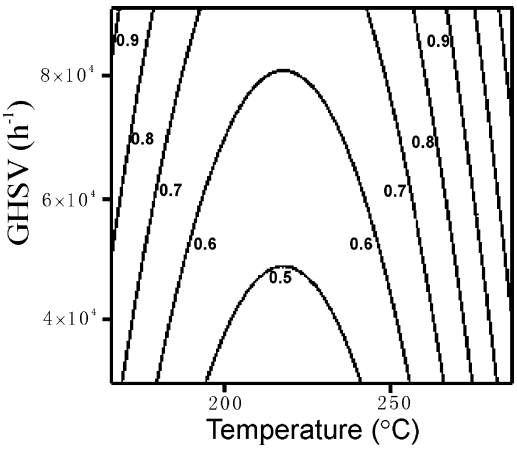

Figure 4. Contour plot of NO_x selectivity versus temperature and GHSV.

might include reactor shape, catalyst shape, Pt concentration in the catalyst, and other catalyst-related properties.

3.2.2. Effects of Temperature and GHSV on C_3H_6 Conversion. Although C_3H_6 conversion was not our main concern, it is important to know how temperature and GHSV affect C_3H_6 conversion because excessive hydrocarbon emissions are also harmful to the environment. A regression analysis for C_3H_6 conversion (y_2), similar to that described above, was also performed. The results showed that X_4^2 and X_3X_4 were not significant because the p values for these two terms were larger than 0.05. After dropping these two terms, a new regression analysis was done that resulted in the regression equation

$$y_2 = 0.724 + 0.353X_3 - 0.108X_4 - 0.217X_3^2 \qquad (6)$$

An R^2 value of 99.0% was also obtained in this analysis, again indicating that our model explained 99% of the total variability. Also, we found that temperature and GHSV have no interactive effect on C_3H_6 conversion.

The effects of temperature and GHSV on C_3H_6 conversion are given by the contour plot of eq 6 as shown in Figure 3. An excessively high GHSV limits C_3H_6 conversion, preventing high C_3H_6 conversion regardless of the reaction temperature. As discussed above, we consider that the rollovers at high temperature in these curves are caused by artifacts. That conclusion is supported by other experiments (not shown here) in which C_3H_6 conversion reached a high constant value around 95% with a GHSV of 30 300 h^{-1}. These curves, produced by our model, would be improved if more data were taken between the transition temperature and 287 °C. Such a conclusion is common when using mathematical models derived from a face-centered-cube design: Some unphysical curvature near the edges of the data region might need to be adjusted, and this can be fixed by taking more data in the edge region. A comparison of Figures 2 and 3 shows that a lower C_3H_6 conversion than HCN conversion was obtained at the same temperature and GHSV values, but both reactions follow the same general behavior.

3.2.3. Effects of Temperature and GHSV on NO_x Selectivity. NO_x selectivity was also investigated because NO_x is undesirable in engine exhaust, and platinum is known to have lean-NO_x activity. Results from the regression analysis for NO_x selectivity (y_3) suggest that the terms X_4^2 and X_3X_4 were not significant. After these two terms had been dropped, a new regression equation was obtained with an R^2 value of 96.3%

$$y_3 = 0.544 + 0.116X_3 + 0.403X_3^2 + 0.0955X_4 \qquad (7)$$

The effects of temperature and GHSV on NO_x selectivity are given by the contour plot of eq 7 after X_3 and X_4 have been replaced by eqs 3 and 4, as shown in Figure 4. NO_x selectivity depends on the temperature more strongly than on the GHSV value. NO_x selectivity is below 100% throughout most of region of the experimental parameters. High values for the temperature and GHSV caused NO_x selectivities larger than 100% to be observed. This simply means that the NO_x concentration in the effluent is larger than that in the influent, and this is understandable because some HCN is converted to NO_x. This occurs because of the following reactions that are typical in our experiments:[17] (1) NO is reduced by HCN to produce N_2O and N_2; (2) HCN is oxidized to N_2, N_2O, NO, and NO_2 with different selectivities at different temperatures; and (3) NO is oxidized to NO_2. High values for GHSV and low temperature allow NO to pass the catalyst without much reduction, and this causes high selectivity for NO_x. High temperatures lead to high conversions of HCN to NO_x, which also leads to high NO_x selectivity. Low NO_x selectivity occurs at low values of GHSV and temperatures around 215 °C.

4. Conclusions

We have shown by using a fractional factorial experimental design that NO and C_3H_6 concentrations have no major effects on HCN conversion in HCN oxidation reactions over a supported platinum catalyst under lean-burn conditions. The fractional factorial design approach demonstrated that the important factors in HCN conversion under these conditions were the reaction temperature and the gas hourly space velocity (GHSV) and also the interaction effects between these two factors. Central composite design was then used in a detailed study of the effects of temperature and GHSV on HCN conversion, C_3H_6 conversion, and NO_x selectivity. The results show that HCN conversion was strongly affected by temperature in both a linear term and a polynomial term, by GHSV in a linear term, and by a temperature−GHSV interaction. Both C_3H_6 conversion and NO_x selectivity were strongly affected by temperature in both a linear term and a polynomial term and by GHSV in a linear term, with no interaction effects between temperature and GHSV found. Low NO_x selectivity was found at low GHSV values near a temperature of 215 °C.

Acknowledgment

Acknowledgment is made to the U.S. Department of Energy, Office of Energy Efficiency and Renewable Energy, FreedomCAR and Vehicle Technologies (DOE/OFCVT), for

support of this program. The work was performed as part of a CRADA with the USCAR Low Emissions Technologies Research and Development Partnership (LEP), Pacific Northwest National Laboratory (PNNL), and DOE/OFCVT. The research described in this paper was performed at the Environmental Molecular Science Laboratory, a national scientific user facility located at PNNL. PNNL is operated for the U.S. DOE by Battelle Memorial Institute under Contract No. DEAC0676RLO1831. B.E.K. acknowledges support by the Department of Energy, Office of Basic Energy Sciences, Chemical Sciences Division.

Literature Cited

(1) Yoon, S.; Panov, A. G.; Tonkyn, R. G.; Ebeling, A. C.; Barlow, S. E.; Balmer, M. L. An examination of the role of plasma treatment for lean NO_x reduction over sodium zeolite Y and gamma alumina. *Catal. Today* **2002**, *72*, 243.

(2) Hoard, J. W.; Panov, A. G. *Products and Intermediates in Plasma-Catalyst Treatment of Simulated Diesel Exhaust*; SAE Technical Paper 2001-01-3512; SAE International: Warrendale, PA, 2001.

(3) Silberova, B.; Burch, R.; Goguet, A.; Hardacre, C.; Holmen, A. Low-temperature oxidation reactions of ethane over a Pt/Al_2O_3 catalyst. *J. Catal*. **2003**, *219*, 206.

(4) Fullerton, D. J.; Westwood, A. V. K.; Brydson, R.; Twigg, M. V.; Jones, J. M. *Catal. Today* **2003**, *81*, 659.

(5) Ordóñez, S.; Bello, L.; Sastre, H.; Rosal, R.; Díez, F. V. Kinetics of the deep oxidation of benzene, toluene, *n*-hexane and their binary mixtures over a platinum on γ-alumina catalyst. *Appl. Catal. B* **2002**, *38*, 139.

(6) Pantu, P.; Gavalas, G. R. Methane partial oxidation on Pt/CeO_2 and Pt/Al_2O_3 catalysts. *Appl. Catal. A* **2002**, *223*, 253.

(7) Klinghoffer, A. A.; Cerro, R. L.; Abraham, M. A. Catalytic wet oxidation of acetic acid using platinum on alumina monolith catalyst. *Catal. Today* **1998**, *40*, 59.

(8) Beretta, A.; Piovesan, L.; Forzatti, P. An Investigation on the Role of a Pt/Al_2O_3 Catalyst in the Oxidative Dehydrogenation of Propane in Annular Reactor. *J. Catal*. **1999**, *184*, 455.

(9) Bourane, A.; Bianchi, D. Oxidation of CO on a Pt/Al_2O_3 Catalyst: From the Surface Elementary Steps to Lighting-Off Tests: II. Kinetic Study of the Oxidation of Adsorbed CO Species Using Mass Spectroscopy. *J. Catal*. **2002**, *209*, 114.

(10) Bourane, A.; Bianchi, D. Oxidation of CO on a Pt/Al_2O_3 Catalyst: From the Surface Elementary Steps to Lighting-Off Tests: III. Experimental and Kinetic Model for Lights-Off Tests in Excess CO. *J. Catal*. **2002**, *209*, 126.

(11) Serre, C.; Garin, F.; Belot, G.; Maire, G. Reactivity of Pt/Al_2O_3 and $Pt-CeO_2Al_2O_3$ Catalysts for the Oxidation of Carbon Monoxide by Oxygen: I. Catalyst Characterization by TPR Using CO as Reducing Agent. *J. Catal*. **1993**, *141*, 1.

(12) Uchisawa, J. O.; Obuchi, A.; Zhao, Z.; Kushiyama, S. Carbon oxidation with platinum supported catalysts. *Appl. Catal. B* **1998**, *18*, L183.

(13) Farrauto, R. J.; Lee, H. C. Ammonia oxidation catalysts with enhanced activity. *Ind. Eng. Chem. Res.* **1990**, *29*, 1125.

(14) Li, Y.; Armor, J. N. Selective NH_3 oxidation to N_2 in a wet stream. *Appl. Catal. B* **1997**, *13*, 131.

(15) Mieher, W. D.; Ho, W. Thermally activated oxidation of NH_s on Pt(111): Intermediate species and reaction mechanisms. *Surf. Sci*. **1995**, *322*, 151.

(16) Burch, R.; Sullivan, J. A. A Transient Kinetic Study of the Mechanism of the $NO/C_3H_6/O_2$ Reaction over $Pt-SiO_2$ Catalysts. *J. Catal*. **1999**, *182*, 489.

(17) Zhao, H.; Tonkyn, R. G.; Barlow, S. E.; Koel, B. E.; Peden, C. H. F. Catalytic oxidation of HCN over a 0.5% Pt/Al_2O_3 catalyst. *Appl. Catal. B* submitted.

(18) Svennberg, H.; Bergh, S.; Stenhoff, H. Factorial design for the development of automated solid-phase extraction in the 96-well format for determination of tesaglitazar, in plasma, by liquid chromatography−mass spectrometry. *J. Chromatogr. B* **2003**, *787*, 231.

(19) Morris, N. D.; Mallouk, T. E. A High-Throughput Optical Screening Method for the Optimization of Colloidal Water Oxidation Catalysts. *J. Am. Chem. Soc*. **2002**, *124*, 11114.

(20) Wen, T. C.; Kuo, H. H.; Gopalan, A. Statistical Design Strategies To Optimize Properties in Emulsion Copolymerization of Methyl Methacrylate and Acrylonitrile. *Ind. Eng. Chem. Res*. **2001**, *40*, 4536.

(21) Subra, P.; Jestin, P. Screening Design of Experiment (DOE) Applied to Supercritical Antisolvent Process. *Ind. Eng. Chem. Res*. **2000**, *39*, 4178.

(22) Chung, T. W.; Lai, C. H.; Wu, H. Evaluation of Process Variables in a Stripping/Regeneration Process Using the Experimental Design Methodology. *Ind. Eng. Chem. Res*. **2000**, *39*, 2519.

(23) Perkins, L. W.; Klasson, K. T.; Counce, R. M.; Bienknowski, P. R. Development of Nitrolysis for Excess Sludge Treatment II: A Factorial Study for Industrial Wastes. *Ind. Eng. Chem. Res*. **2003**, *42*, 5457.

(24) Martin, C.; Cuellar, J. Synthesis of Poly(styrene-*co*-divinylbenzene)-Stainless Steel Beads through a Factorial Design of Experiments. *Ind. Eng. Chem. Res*. **2004**, *43*, 2093.

(25) Mellor, J. R.; Coville, N. J.; Durbach, S. H.; Copperthwaite, R. G. Acid leached Raney copper catalysts for the water−gas shift reaction. *Appl. Catal. A* **1998**, *171*, 273.

(26) Finta, Z.; Hell, Z.; Balán, D.; Cwik, A.; Kemény, S.; Figueras, F. Mg−Al 3:1 hydrotalcite catalyst in the synthesis of cyclopropane carboxylic acid derivatives. *J. Mol. Catal. A* **2000**, *161*, 149.

(27) Aksoylu, A. E.; Önsan, Z. I. Interaction between Nickel and Molybdenum in $Ni-Mo/Al_2O_3$ Catalysts: II: CO Hydrogenation. *Appl. Catal. A* **1998**, *168*, 399.

(28) Chen, H.; Adesina, A. A. Design of a multimetallic catalyst system for hydrocarbon synthesis: A statistical optimisation procedure. *Appl. Catal. A* **1997**, *162*, 47.

(29) Hardiman, K. M.; Cooper, C. G.; Adesina, A. A. Multivariate Analysis of the Role of Preparation Conditions on the Intrinsic Properties of a $Co-Ni/Al_2O_3$ Steam-Reforming Catalyst. *Ind. Eng. Chem. Res*. **2004**, *43*, 6006.

(30) Chen, L. C.; Huang, C. M. Application of Statistical Strategies to Process Optimization of Sol−Gel-Derived SiO_2 Modification of TiO_2. *Ind. Eng. Chem. Res*. **2004**, *43*, 6446.

(31) Box, G. E. P.; Hunter, W. R.; Hunter, J. S. *Statistics for Experimenters*; Wiley: New York, 1978.

(32) Vining, G. G. *Statistical Methods for Engineers*; Duxbury-Brooks/Cole: Pacific Grove, CA, 1998.

Received for review December 19, 2004
Resubmitted for review November 21, 2005
Accepted November 22, 2005

IE048777E